Proton therapy induces a local microglial neuroimmune response

Voshart, Daniëlle C; Klaver, Myrthe; Jiang, Yuting; van Weering, Hilmar R J; van Buuren-Broek, Fleur; van der Linden, Gideon P; Cinat, Davide; Kiewiet, Harry H; Malimban, Justin; Vazquez-Matias, Daniel A

Published in:
Radiotherapy and Oncology

DOI:
10.1016/j.radonc.2024.110117

Publication date:
2024

Radiotherapy and Oncology 193 (2024) 110117

Contents lists available at ScienceDirect

Radiotherapy and Oncology

journal homepage: www.thegreenjournal.com

Original Article

Proton therapy induces a local microglial neuroimmune response

Daniëlle C. Voshart [a,b], Myrthe Klaver [a,b,1], Yuting Jiang [a,b,1], Hilmar R.J. van Weering [c], Fleur van Buuren-Broek [a,b], Gideon P. van der Linden [a,b], Davide Cinat [a,b], Harry H. Kiewiet [d], Justin Malimban [a], Daniel A. Vazquez-Matias [a,b], Luiza Reali Nazario [a,b], Ayla C. Scholma [a,b], Jeffrey Sewdihal [a,b], Marc-Jan van Goethem [a,d], Peter van Luijk [a,b], Rob P. Coppes [a,b], Lara Barazzuol [a,b,*]

[a] Department of Radiation Oncology, University Medical Center Groningen, University of Groningen, Groningen 9700 RB, The Netherlands
[b] Department of Biomedical Sciences, Section of Molecular Cell Biology, University Medical Center Groningen, University of Groningen, Groningen 9700 AD, The Netherlands
[c] Department of Biomedical Sciences, Section of Molecular Neurobiology, University Medical Center Groningen, University of Groningen, Groningen 9700 AD, The Netherlands
[d] Department of Biomedical Sciences, PARTREC, University Medical Center Groningen, University of Groningen, Groningen 9747 AA, The Netherlands

ARTICLE INFO

Keywords:
Photons
Protons
SOBP
Brain
Neuroinflammation
Microglia
Innate immune memory

ABSTRACT

Background and purpose: Although proton therapy is increasingly being used in the treatment of paediatric and adult brain tumours, there are still uncertainties surrounding the biological effect of protons on the normal brain. Microglia, the brain-resident macrophages, have been shown to play a role in the development of radiation-induced neurotoxicity. However, their molecular and hence functional response to proton irradiation remains unknown. This study investigates the effect of protons on microglia by comparing the effect of photons and protons as well as the influence of age and different irradiated volumes.

Materials and methods: Rats were irradiated with 14 Gy to the whole brain with photons (X-rays), plateau protons, spread-out Bragg peak (SOBP) protons or to 50 % anterior, or 50 % posterior brain sub-volumes with plateau protons. RNA sequencing, validation of microglial priming gene expression using qPCR and high-content imaging analysis of microglial morphology were performed in the cortex at 12 weeks post irradiation.

Results: Photons and plateau protons induced a shared transcriptomic response associated with neuro-inflammation. This response was associated with a similar microglial priming gene expression signature and distribution of microglial morphologies. Expression of the priming gene signature was less pronounced in juvenile rats compared to adults and slightly increased in rats irradiated with SOBP protons. High-precision partial brain irradiation with protons induced a local microglial priming response and morphological changes.

Conclusion: Overall, our data indicate that the brain responds in a similar manner to photons and plateau protons with a shared local upregulation of microglial priming-associated genes, potentially enhancing the immune response to subsequent inflammatory challenges.

Introduction

Neurocognitive sequelae are the leading cause of a reduced quality of life in paediatric and adult primary brain and central nervous system tumour patients [1]. In addition, patients with brain metastases also experience debilitating neurocognitive impairment [2]. Although radiotherapy is an integral part of the treatment of brain tumours, it is associated with the development of neurocognitive side effects due to the co-irradiation of normal brain tissue [3]. Despite the introduction of 3D conformal radiotherapy and intensity-modulated radiotherapy, preventing or minimising radiotherapy-induced neurocognitive sequelae remains a pressing need [4].

One such preventative effort is proton therapy, the use of which has increased rapidly over the past decade, particularly in paediatric patients [5]. Unlike conventional photons (X-rays), protons deposit most of their energy close to the end of the range in the so-called Bragg peak.

* Corresponding author at: Hanzeplein 1, Groningen 9713 GZ, The Nederlands.
E-mail address: l.barazzuol@umcg.nl (L. Barazzuol).
[1] These authors contributed equally.

https://doi.org/10.1016/j.radonc.2024.110117
Received 15 June 2023; Received in revised form 25 January 2024; Accepted 28 January 2024
Available online 6 March 2024

This allows a substantial reduction in the dose to the normal brain tissue outside the target tumour volume. While the spread-out Bragg peak (SOBP) region covers the tumour volume, the normal tissue is mostly exposed to plateau protons and only a small portion of normal tissue might receive SOBP protons [6]. Despite the clear physical advantage of proton therapy, there are still significant uncertainties as to whether there is a differential biological response of the normal brain to protons [7]. In the clinic, a relative biological effectiveness (RBE) of 1.1 is currently used in proton treatment planning to account for the increased Linear Energy Transfer (LET) in the SOBP. However, the RBE has been shown to vary substantially between experiments depending on the biological endpoint, dose and LET, and has been mostly based on clonogenic survival data, which are not the only relevant indicator for late side effects [7]. Moreover, a growing number of studies report an increase in MRI contrast-enhancing brain lesions after proton therapy [8–10]. These observations indicate that there might be differences in underlying biological responses to photons and protons in the brain, besides dose modification. This highlights the need for pre-clinical studies comparing the responses to both radiation types.

Previous studies have shown that neuroinflammation and its orchestration by microglia, the resident immune cells of the brain, contribute significantly to cognitive decline after brain irradiation [11–13]. Microglia can become reactive after radiation exposure, which can disrupt neuroplasticity, among other responses [14]. Importantly, we have recently shown that brain irradiation with single and fractionated photon doses can modulate the innate immune memory (IIM) of microglia by leading to persistent molecular reprogramming of microglia into a primed state [15]. Primed microglia are characterised by distinct molecular and morphological changes, which functionally lead to an exaggerated immune response when exposed to secondary inflammatory insults [16]. This exaggerated response is thought to contribute to the pathogenesis of neurogenerative diseases [16,17]. However, whether proton irradiation induces microglial priming to the same degree as photons and whether this radiation-induced microglial response is local and can be spatially minimised by reducing the irradiated volume remain important questions to be addressed.

In this study, we performed comparative transcriptomic and tissue analysis of rats irradiated locally to the whole brain with photons, plateau and SOBP protons. Irradiation with photons and plateau protons induced comparable microglial priming gene expression and morphological changes. Microglial priming gene expression was slightly higher after irradiation with SOBP protons and age dependent. Furthermore, high-precision proton irradiation to the 50 % anterior or 50 % posterior brain volumes showed that these microglial molecular and morphological changes are local.

Methods

Animals

The study was performed on male Wistar (Hsd/Cpb:WU) rats that were kept under environmentally controlled conditions (temperature: 21 °C, humidity: 55 %) and a 12 h light/dark cycle (light 08:00–20:00 in winter and 07:00–19:00 in summer) with ad libitum chow and water. The animals were housed in groups in open cages, except for the animals irradiated at 4 weeks of age and their controls (juveniles), who were housed in pairs in individually ventilated cages (IVC) during the whole study. Animals were also housed in pairs in IVC from one week prior to proton irradiation until 5 weeks after proton irradiation. The animal procedures were performed at the UMCG Central Animal Facility according to the guidelines from Directive 2010/63/EU of the European Parliament on the protection of animals used for scientific purposes. The experiments were approved by the Central Authority for Scientific Procedures on Animals (CCD) (license # AVD1050020184808) and the Animal Care and Use Committee of the University of Groningen.

Irradiation

Rats were irradiated with 14 Gy photons or protons. According to the biologically effective dose equation [18], a 14 Gy single dose is equivalent to a clinically relevant dose of 56 Gy given in 2 Gy fractions (α/ß value of 2). Photon irradiations were performed in the Central Animal Facility of the UMCG and proton irradiations were performed at the Particle Therapy Research Center (PARTREC) accelerator facility of the UMCG. Proton irradiated animals and their controls were housed at PARTREC from 1 week prior until 2 days post irradiation. Rats were anesthetised using isoflurane (5 % induction, 1.5–2 % maintenance), placed in a holder hanging on a positioning rod by their upper incisors (for more details see [19–21]). This allowed for the precise irradiation of the whole or partial brain through a specialised collimator located on the dorsal side of the animal's head (Fig. S1A-C) [22]. Rats were irradiated to the whole brain with 14 Gy X-ray photons (X-RAD 320, Precision X-Ray inc, operated at 200 kV at 1.559 Gy/min)[22,23], plateau protons (scattered beam, 150 MeV shoot-through, operated at 15 Gy/min) [20] or SOBP protons (4 Gy/min, Fig. S1D). The proton dose rates were maximised under standard conditions to ensure efficient execution of the experiment and to have a similar time under anaesthesia per animal as during the photon irradiation. The plateau proton dose rate was the highest we could achieve within radiation safety constraints and the SOBP dose rate was the highest we could technically achieve while still maintaining high uniformity of the dose distribution. Although the plateau proton dose rate is slightly higher than clinical dose rates, the biological response of normal tissues is expected to be similar within these dose rate levels [24]. The SOBP with a 4 cm modulation length was produced from the same beam by varying the thickness of an aluminium range shifter (Table S1). Additional aluminium range shifter material was used to position the SOBP so that it covered the entire brain of the rats. 50 % Anterior or 50 % posterior brain sub-volumes were irradiated with 14 Gy plateau protons (150 MeV, operated at 15 Gy/min). The same anaesthesia procedure was followed for the sham-irradiated controls. Adult rats were irradiated at 9 weeks of age (adult, mean weight: 310 g ± SD 24.4). Juvenile rats were irradiated at 4 weeks of age (juvenile, age: P28, mean weight: 92 g ± SD 7.0). We have previously found that microglial priming is persistent up to a year after photon irradiation [15] and have here conducted the study at 12 weeks post irradiation. Animals were sacrificed at 12 weeks post irradiation by saline perfusion under dexmedetomidine-ketamine anaesthesia. The brains were isolated and divided in two hemispheres. These hemispheres were either fixed in 4 % paraformaldehyde for 48 h and embedded in paraffin or dissected and snap frozen.

RNA isolation and RNA sequencing

For total RNA isolation, 15 × 40 μm thin sections were cut from the snap frozen anterior cortex per animal and processed using the RNeasy Lipid Tissue Mini kit (Qiagen, cat#74804) according to the manufacturer's instructions. RNA sequencing (RNA-seq) was performed on 3 controls, 3 photon and 3 proton-irradiated animals at 12 weeks post irradiation. Quality of the RNA was determined using Agilent ScreenTape System, all samples had a RIN > 7.7. Library preparation was performed with the Lexogen QuantSeq 3′ mRNA-Seq Library Prep Kit (FWD) using 200 ng RNA per sample. All libraries were pooled equimolarly and sequenced on a NextSeq 500 at the research sequencing facility of the UMCG.

RNA sequencing data analysis

The data was aligned to the rat genome Rnor_6.0.93 and preprocessed using the Lexogen Quantseq 2.3.1 FWD UMI pipeline. Downstream analysis was performed in Rstudio (v4.0.3) where the package edgeR (v3.36.0) [25] was used for normalisation and differential gene expression analysis. Differentially expressed genes (DEGs)

Table 1
Animal group size per experiment.

Analysis	Figures	Treatment groups	Animal number per group
RNA sequencing	1A-D	Control, photon and proton	3
qPCR of microglial priming genes	1E, S2A	Control, photon, plateau proton, SOBP proton	5
qPCR of microglial priming genes	1F, S2B	Juvenile control, juvenile proton, adult control, adult proton	5
Microglial density and morphology in the anterior cortex	2, S3	Control, photon, plateau proton	6
qPCR of microglial priming genes	3B, S4	Control, whole brain, 50 % anterior, 50 % posterior	5
Microglial density in the anterior cortex	3D	Control, whole brain, 50 % anterior, 50 % posterior	6
Microglial morphology in the anterior cortex	3E-H, S5	Control, whole brain, 50 % anterior, 50 % posterior	5 for the control group, 6 for the other groups
Microglial density in the colliculus inferior	S6C	Control, whole brain, 50 % anterior, 50 % posterior	6 for the 50 % anterior group, 5 for the other groups
Microglial morphology in the colliculus inferior	S6D-G	Control, whole brain, 50 % anterior, 50 % posterior	6 for the 50 % anterior group, 5 for the other groups

were detected using a threshold of $\log_2$FC > 0.59 and FDR < 0.05. PCA plots were generated in Rstudio using ggplot2 (v3.4.2) [26] and used to check for correlation with library size. Plots were made with Pheatmap (v1.0.12) [27] and ggplot2. Gene ontology (GO) enrichment analysis and gene set enrichment analysis (GSEA) were performed by using clusterProfiler (v3.0.4) [28] and the database "GO_Biological_Process_2018" was used to find enriched GO terms, which were considered significant if they had an adjusted P value < 0.05.

cDNA synthesis and qPCR

cDNA was transcribed from RNA using M−MLV reverse transcriptase (Invitrogen, cat#28025013) according to the manufacturer's instructions. Quantitative PCR (qPCR) was performed in triplicate using iQ SYBR Green Supermix (Bio-Rad, cat#170-8885) on a Bio-Rad real-time PCR system. Relative mRNA expression was calculated with the $2^{-\triangle\triangle CT}$ method using *Ywhaz* as internal control. Primer sequences are listed in Table S2.

Immunohistochemistry

10 μm paraffin sections of rat brain samples were dewaxed and rehydrated. Antigen retrieval was performed by boiling the sections for 12 min in 10 mM sodium citrate in demiwater at pH 6. After washing three times with phosphate buffered saline (PBS) (identical for subsequent washing steps), endogenous peroxidase was blocked with 0.3 % H_20_2 for 30 min. The sections were washed and blocked with 5 % donkey serum (Jackson Immuno Research, cat#017-000-121) in PBS+ (PBS with 0.3 % Triton X-100) for 1 h and were then incubated with the primary antibody rabbit anti-ionized calcium-binding adapter molecule 1 (IBA1) (WAKO, cat#019-19741, 1:1000) overnight at 4 °C. After washing, the samples were incubated with the biotinylated secondary donkey-α-rabbit IgG antibody (1:400; Jackson Immuno Research, cat#711-065-152) in PBS+ for 1 h. The sections were washed, incubated with avidin–biotin complex solution (VECTASTAIN® ABC Kit, Vector Laboratories, cat#PK-6100) for 30 min and washed again. The sections were then stained with 0.04 % 3,3′-Diaminobenzidine (Merck, cat#D5637) in PBS with 0.01 % H_2O_2 for 10 min and subsequently dehydrated with increasing ethanol concentrations. The slides were air-dried for 30 min, mounted with coverslips using DePex (Serva, cat#18243.01) and stored at room temperature.

Imaging and density measurement

The slides were scanned with the NanoZoomer 2HT 2.0 digital slide scanner (Hamamatsu Photonics) at 40× magnification and saved as user-blinded NDPI files. The staining was performed with 6 animals per group; however, some blinded NDPI files were excluded when the staining or imaging quality was not sufficient. Group sizes are provided in Table 1. Microglia densities were determined in the frontal cortex and the colliculus inferior. The number of IBA1-positive cells in these areas were counted using ImageJ manual cell counting. For the anterior cortex, three 1 mm^2 squares were assessed per animal and the average microglia density per 1 mm^2 was calculated (n = 6 animals per group). For the colliculus inferior, one 1 mm^2 square was assessed per animal (n = 5–6 animals per group).

Morphometric analysis of microglia

The NDPI scans were user-blinded and single cell images of microglia in the rat anterior cortex (which is irradiated in the 50 % anterior group) and colliculus inferior (which is irradiated in the 50 % posterior group) were extracted and processed for morphometric analysis as described previously [29]. In total, 25 cells per region per animal were selected for analysis, with 5 or 6 animals per group. Cells were randomly selected with the following cell selection criteria: containing a soma and not having clear interruptions in branches. The output of the morphometric analyses consisted of 25 morphometric features, a Sholl analysis, and two fractal analyses to determine the fractal dimension and lacunarity. A list of features and definitions can be found in Table S3. A hierarchical clustering on principal components (HCPC) approach was applied to each morphometric data set to allow categorization and comparison of microglia morphologies between experimental groups. In short, the features were normalized to ensure close-to-normal distribution (-0.5 > skewness > 0.5) and the data was subsequently scaled and centered by a Z-transform. A principal component was applied on the normalized data and principal components (PCs) with an eigenvalue > 1 were retained for agglomerative hierarchical clustering following Ward's method [30]. The distribution of microglia over the respective clusters (in percentage) was determined and compared between experimental conditions. The analyses were performed separately for Fig. 2, Fig. 3 and Fig. S6.

Statistical analyses

Statistical analyses were performed with GraphPad Prism 8 (GraphPad Software Inc.). Animal numbers per group are also shown in Table 1. For the microglial priming gene comparisons of Fig. 1E, 3B, Fig. S2A and S4, a one-way ANOVA was used and for the comparison of Fig. 1F and Fig. S2B, a two-way ANOVA was used. These ANOVAs were followed by Tukey's multiple comparisons tests with log2 transformed data (n = 5). For the comparisons of microglial cell density (Fig. 3D, Fig. S6, n = 5–6) and the contribution of homeostatic and reactive clusters between groups (Fig. S3D, n = 6), a one-way ANOVA followed by Tukey's multiple comparisons test was used. All statistical details are also provided in the relative Figure legends. We defined a p-value less than 0.05 as statistically significant.

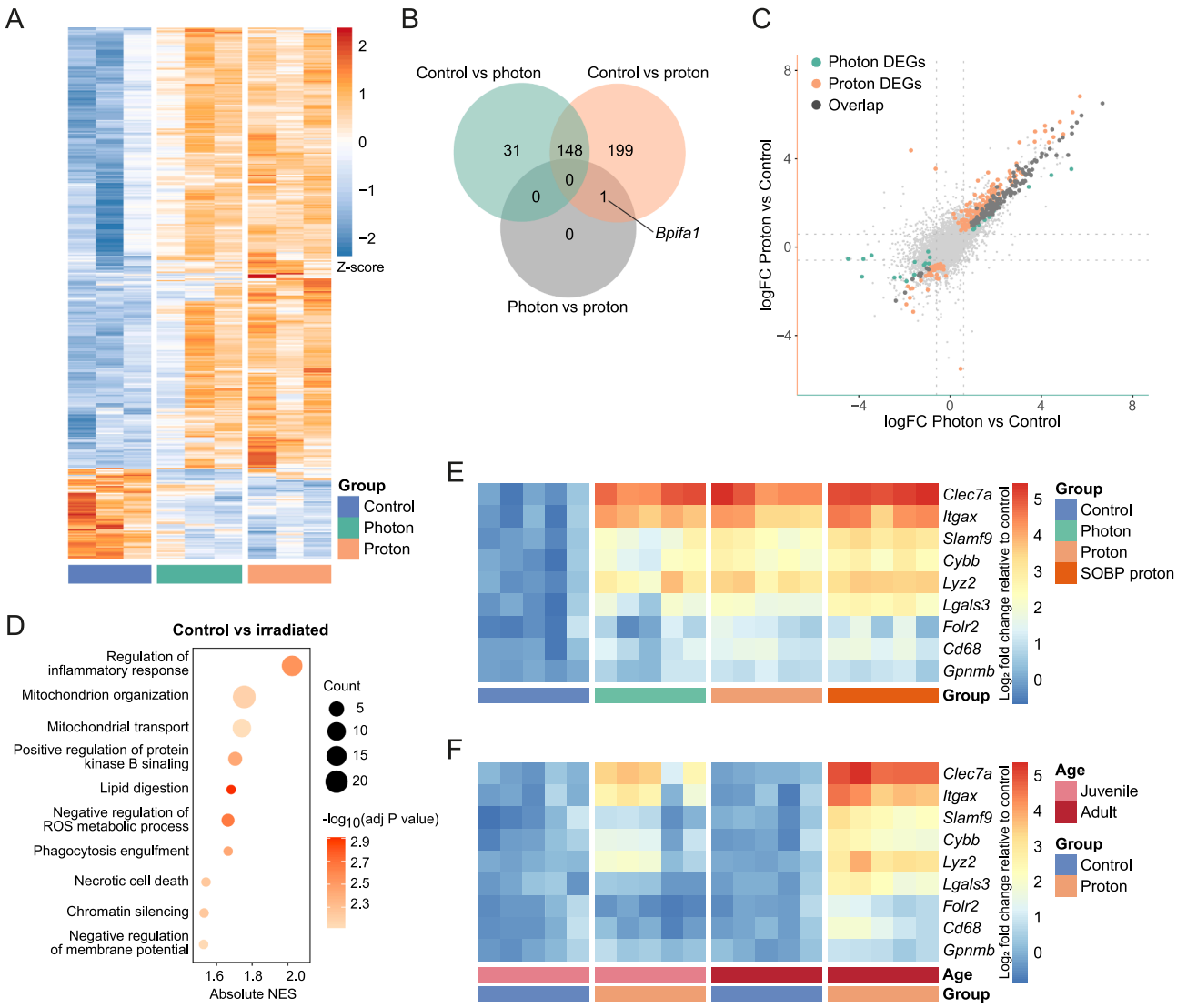

Fig. 1. Identification of a shared neuroinflammatory response after photon and proton irradiation. (A) Rats were irradiated to the whole brain with 14 Gy X-ray photons (photon) or plateau protons (proton) and bulk RNA sequencing in cortical samples was performed at 12 weeks post irradiation. The heatmap depicts the differentially expressed genes (DEGs) (fold change (FC) > 1.5, false discovery rate (FDR) < 0.05) between the groups. $n = 3$ animals per group. (B) Venn diagram of the number of DEGs between groups. (C) Four-way plot showing overlapping DEGs (dark grey) between photon vs control (green) and proton vs control (orange) data sets, determined on the basis of FC > 1.5 and FDR < 0.05. Genes that are not differentially expressed between any of the groups are depicted in light grey. (D) Gene ontology (GO) analysis of DEGs between control and all photon and proton samples combined. $n = 3$ animals per group for control, $n = 6$ animals per group for irradiated. (E) Heatmap depicting gene expression of 9 microglial priming genes of rats irradiated to the whole brain with 14 Gy X-ray photons (photon), plateau protons (proton), or SOBP protons (SOBP proton). $n = 5$ animals per group. (F) Animals irradiated as juvenile (4 week-old) or adult (9 week-old) to the whole brain with 14 Gy plateau protons. Colours in panel E and F indicate $\log_2$ transformed fold change relative to corresponding controls. $n = 5$ animals per group. See also Fig. S2 for further details and statistics. (For interpretation of the references to colour in this figure legend, the reader is referred to the web version of this article.)

Results

To determine the transcriptional changes induced by photon and proton brain irradiation, bulk RNAseq was performed on cortical samples isolated from rats at 12 weeks after whole brain irradiation with either 14 Gy of photons (X-rays) or plateau protons (150 MeV shoot-through; for further details see Methods). We found a total of 378 differentially expressed genes (DEGs) between control, photon and proton irradiated samples (Fig. 1A, B, Table S4). Photons and protons induced a similar transcriptomic response with 148 shared DEGs when compared to control, and only 1 DEG (*Bpifa1*) found when comparing photons and protons (Fig. 1B, C). Gene ontology (GO) analysis of the DEGs between control and both irradiated groups showed enrichment for biological processes related to the regulation of inflammatory responses, and mitochondrial organization and transport (Fig. 1D). The most significantly expressed DEG between irradiated and control animals was *Clec7a*, a previously established microglial priming gene (Table S4) [31]. To further investigate the effect of protons and photons on microglial priming, we performed qPCR using 9 known microglial priming signature genes on cortical tissues isolated from photon, plateau proton and SOBP proton irradiated animals. SOBP protons were generated as described in the Methods. Both photons and plateau protons induced a similar increased expression of microglial priming genes. Whereas SOBP proton irradiated animals showed a slight overall increase in microglial priming gene expression compared to photon or plateau proton irradiated animals, being statistically significant for *Slamf9* and *Lgals3* (Fig. 1E, Fig. S2A).

Since age can affect this response [15] and paediatric brain tumour

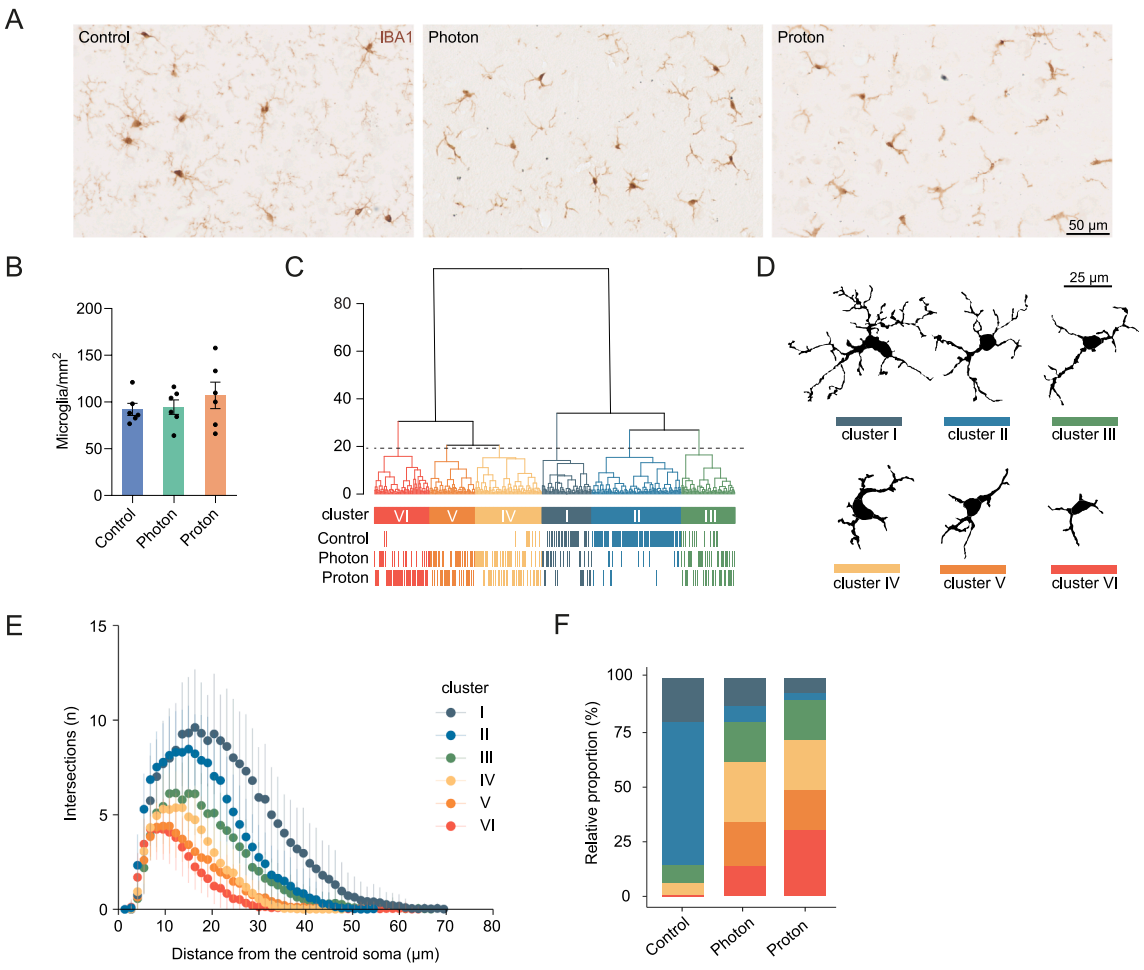

Fig. 2. Similar microglial cell density and morphologies after photon and proton irradiation. (A) Representative images and (B) density of microglia (IBA1, brown) in the anterior cortex of control, 14 Gy photon irradiated (photon) and 14 Gy plateau proton irradiated (proton) animals. Bar graph shows mean ± SEM. $n = 6$ animals per group. (C) Dendrogram showing hierarchical clustering of all 450 microglia into 6 clusters. The dashed line indicates the cut-off for the clustering. The horizontal axis shows the 3 different groups, with each line representing an individual cell. The vertical axis shows squared Euclidian distance to show the linkage distance. The different clusters are indicated by colour. (D) Representative silhouettes of microglia from each of the 6 clusters. (E) Sholl plots, each coloured line represents one cluster (mean ± SD). (F) Relative proportion of the different clusters for the control, photon and proton groups. Cluster I-VI are indicated by colour and stacked from top to bottom. n = 6 animals per group, with 25 microglia per animal. For the comparisons of microglial cell density, a one-way ANOVA followed by Tukey's multiple comparisons test ($n = 6$) was used. See also Fig. S3 for further details. (For interpretation of the references to colour in this figure legend, the reader is referred to the web version of this article.)

patients are often treated with proton therapy [5], we also performed this analysis on juvenile animals irradiated with plateau protons at post-natal day 28 (P28). While there was a significant increase in some of the microglial priming genes in juvenile irradiated animals compared to control, the overall increase was less pronounced than in adults (Fig. 1F, Fig. S2B). Together, these data suggest that brain irradiation with plateau protons induces transcriptomic changes and microglial priming to a similar degree as photons and that this priming response is age-dependent and slightly increased after SOBP protons.

Alongside molecular changes, the response of microglia to damage is often accompanied by changes in cell proliferation and morphology. Therefore, we determined microglial cell densities and performed high-content imaging analysis of microglial morphology in the frontal cortex of photon and plateau proton irradiated rats. At 12 weeks post-irradiation, microglial cell density in the cortex was similar in the photon and proton irradiated groups when compared to controls (Fig. 2A, B). Morphological categorization of cortical microglia by hierarchical clustering on principal components [29] identified 6 clusters, each represented by a distinct microglial morphology, here also called morphologies (Fig. 2C). The majority of microglia in the control animals were categorized in cluster I and II. Cells in these clusters are relatively large and display elaborate branching, a shape which is indicative of homeostatic microglia (Fig. 2D, E, F, Fig. S3). Photon- and proton-irradiated cortical samples contained significantly higher proportions of cells in clusters III-VI, which are characterized by cells with a relatively large cell convexity and smaller cell spread and branch length, indicative of reactive microglia (Fig. 2D, E, F, Fig. S3). No significant differences in the distribution of microglial morphologies were observed between photon and proton irradiated animals (Fig. S3D), indicating that photons and protons lead to similar microglial morphological changes.

To determine whether the observed radiation-induced microglial molecular and morphological changes are local or extend outside the irradiated volume, we performed high-precision proton partial brain irradiation with 14 Gy to the whole brain, 50 % anterior and 50 % posterior sub-volumes of the rat brain (Fig. 3A, Fig. S1A-C). Genes associated with microglial priming were highly expressed in the anterior cortex of the whole brain and 50 % anterior brain irradiated groups, where the cortex was irradiated. Interestingly, 50 % anterior brain irradiated animals also showed a significant increase in two priming

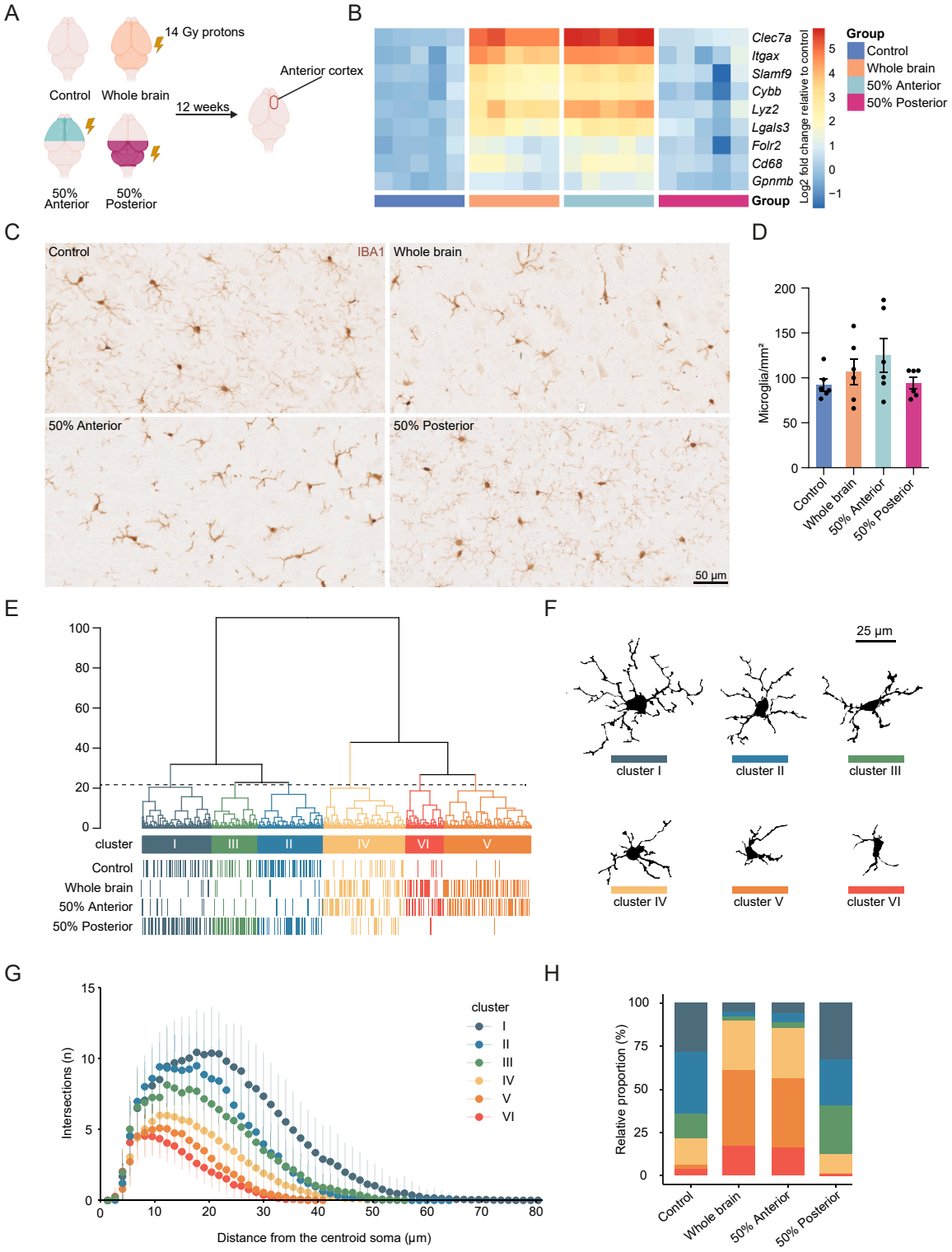

Fig. 3. Local microglia-associated changes after partial brain proton irradiation. (A) Experimental setup. Animals were irradiated to the whole brain, 50 % anterior or 50 % posterior sub-volumes of the brain with 14 Gy plateau protons. At 12 weeks post irradiation, gene expression analysis, microglial cell density and morphometric analyses were performed in the anterior cortex. (B) Heatmap depicting gene expression of 9 microglial priming genes in the different groups. Colours indicate log2 transformed fold change relative to control. $n = 5$ animals per group. (C) Representative images and (D) density of microglia (IBA1, brown) in the anterior cortex of the different groups. Bar graph shows mean ± SEM. $n = 6$ animals per group. (E) Dendrogram showing hierarchical clustering of all 575 microglia into 6 clusters. The dashed line indicates the cut-off for the clustering. The horizontal axis shows the 4 different groups, with each line representing an individual cell. The vertical axis shows squared Euclidian distance to show the linkage distance. The different clusters are indicated by colour. (F) Representative cell silhouettes of microglia from each of the 6 clusters. (G) Sholl plots, each coloured line represents one cluster (mean ± SD). (H) Relative proportion of the different clusters for different groups. Cluster I-VI are indicated by colour and stacked from top to bottom. $n = 5$–6 animals per group, with 25 microglia per animal. For the comparisons of microglial cell density, a one-way ANOVA followed by Tukey's multiple comparisons test ($n = 6$) was used. See also Fig. S4 and S5 for further details and statistics. (For interpretation of the references to colour in this figure legend, the reader is referred to the web version of this article.)

genes when compared to whole brain irradiated animals (Fig. 3B, Fig. S4). This is consistent with the slightly higher, although not statistically different, number of microglia in the cortex of the 50 % anterior irradiated group compared to whole brain irradiated group (Fig. 3C, D). In contrast, microglial priming gene expression was very similar in 50 % posterior brain irradiated animals, of which the cortex was not irradiated, in comparison to control (Fig. 3B, Fig. S4).

Microglial morphometric analysis of the anterior cortex revealed an equal distribution of microglial morphologies in the cortex of whole brain and 50 % anterior irradiated groups, indicating that these morphological changes are not dependent on the size of the irradiated volume (Fig. 3E-H, Fig. S5). The distribution of morphologies in the cortex of the 50 % posterior irradiated group did not differ from control, indicating that radiation-induced microglial morphological changes are local to the irradiated area (Fig. 3H, Fig. S5). Similarly, the colliculus inferior, a region irradiated in the whole brain and 50 % posterior groups, showed morphological changes only in the groups where the colliculus inferior was irradiated (Fig. S6). These results show that protons lead to a neuroinflammatory response resulting in local microglial molecular and morphological changes.

Discussion

Microglia have been shown to play a significant role in the development of radiation-induced neurotoxicity and consequential neurocognitive dysfunction [11,12,14]. However, the effect of protons on the molecular and functional state of microglia remains unclear. Here, we found that photons and plateau protons induce similar transcriptomic and microglial morphological changes in the rat cortex. Analogously to photons [15], proton irradiation leads to an immunological response referred to as priming, in which microglia develop IIM and show a stronger immune response to subsequent inflammatory stimuli. The exaggerated response of primed microglia to systemic inflammation is thought to contribute to the pathogenesis of neurogenerative diseases [16,17], and might therefore also mediate the development of radiation-induced side effects and worsening of pre-existing neuro-toxicities. The microglial priming gene signature depends on the age at the time of irradiation with lower expressions in juvenile animals irradiated with protons in line with our previous study using photons [15]. Importantly, partial brain proton irradiation showed that the observed microglial changes are local to the irradiated area.

Several clinical studies have investigated the effects of proton therapy in brain cancer patients, largely focusing on imaging changes and cognitive outcome [8–10,32–34], highlighting the many biological uncertainties on the effect of protons on the normal brain. In contrast, the number of preclinical studies directly comparing the biological effects of both photons and protons on the normal brain tissue is very limited. Tang *et al.* [35] irradiated juvenile rats to the brain with 10 Gy photon and the same RBE–weighted dose of SOBP proton irradiation and found no significant differences in cognitive, imaging and histological changes, including microglial cell density. Our data show a slight increase in microglial priming gene signature expression in SOBP proton-irradiated animals compared to animals irradiated with photons using the same physical, non RBE-weighted dose. This finding supports RBE adjustments for the SOBP. The radiobiological effect of protons in the plateau region, which is most relevant for the normal tissue, is generally not considered to be different from photons [36]. Our observations concerning microglia are in line with these previous findings. The present difference between plateau and SOBP protons, together with evidence that microglial priming also happens in cancer patients [15], further highlights the potential of proton therapy with a variable RBE-optimised treatment plan.

Protons allow for greater precision in dose delivery and hence better sparing of normal brain tissue. Here, we found that proton-induced microglial priming and morphological changes are present only in the irradiated field and are likely determined by changes in the microenvironment. This indicates that microglia-associated neurotoxicity could be avoided in the parts of the normal brain that are not irradiated and thus the better dose distribution of proton therapy could potentially translate into a distinct biological advantage over conventional photon-based radiotherapy. Additionally, proton therapy can allow selective sparing of brain structures especially vulnerable to radiation-induced toxicities or associated with cognitive outcome, for example the hippocampus [37,38]. This emphasises the importance of further investigation into which brain regions contribute most to radiation-induced cognitive decline.

Although microglial priming does not seem to occur in non-irradiated areas, this research also indicates that the degree of local microglial priming is not decreased when the radiation volume is reduced, underlining the importance of further research into decreasing radiation-induced microglial priming. This closely relates to current immunotherapy efforts, aimed at decreasing the number and activation status of tumour-associated microglia and macrophages, for which several strategies are presently being tested [39]. Moreover, *in vivo* research into the functional effect of an exaggerated immune response and the possible rescue by temporarily using anti-inflammatory agents during an inflammatory insult should be investigated. As an exaggerated immune response of previously primed microglia could possibly contribute to the worsening of side effects in brain cancer patients, we propose that inflammatory insults, such as infections, and the presence of immune-related diseases should be closely monitored during the long term follow up of brain cancer patients as well as in clinical trials investigating the neurocognitive effect of brain irradiation with proton therapy.

Together, our results show that proton brain irradiation induces a similar molecular and morphological microglial response as photons and, importantly, that this is localised to the irradiated region. This underscores the importance of proton therapy, the development of efforts to spare more of the normal brain and therapeutic approaches to ameliorate microglia-induced neurotoxicity.

CRediT authorship contribution statement

Daniëlle C. Voshart: Formal analysis, Investigation, Methodology, Visualization, Writing – original draft, Conceptualization, Writing – review & editing, Project administration. **Myrthe Klaver:** Formal analysis, Methodology, Investigation. **Yuting Jiang:** Formal analysis, Investigation, Visualization, Methodology. **Hilmar R.J. van Weering:** Formal analysis, Resources, Software, Visualization. **Fleur van Buuren-Broek:** Investigation, Methodology. **Gideon P. van der Linden:** Investigation. **Davide Cinat:** Formal analysis. **Harry H. Kiewiet:** Investigation. **Justin Malimban:** Methodology, Validation. **Daniel A. Vazquez-Matias:** Resources. **Luiza Reali Nazario:** Resources. **Ayla C. Scholma:** Investigation. **Jeffrey Sewdihal:** Investigation. **Marc-Jan van Goethem:** Investigation, Methodology, Formal analysis, Writing – review & editing. **Peter van Luijk:** Formal analysis, Methodology, Supervision, Writing – review & editing. **Rob P. Coppes:** Methodology, Supervision, Writing – review & editing. **Lara Barazzuol:** Conceptualization, Funding acquisition, Methodology, Project administration, Supervision, Visualization, Writing – original draft, Writing – review & editing.

Declaration of competing interest

The authors declare the following financial interests/personal relationships which may be considered as potential competing interests: L. B. received funding from Ion Beam Applications (IBA) within the ZonMw Off Road grant (project number 451001001); however, the company did not have any input and interpretation on the design of experiments and the data. The remaining authors declare that they have no conflict of interest.

Acknowledgements

This work was supported by KWF Kankerbestrijding (project numbers 11148 to L.B.), ZonMw Off-Road and IBA (project number 451001001 to L.B.), SU2C-CRUK Pediatric Cancer New Discoveries Challenge Team Grant (project number SU2C#RT6186 to L.B.) and the China Scholarship Council (project number 201906320080 to Y.J.). The authors would like to thank Uilke Brouwer and Julia Wiedemann for their help during irradiations and Tjalling W. Nijboer for the use of Miasuite. We would also like to thank the central animal facility at the UMCG for animal support and the PARTREC operators for their help during irradiations. Some figures were created using BioRender.com.

Appendix A. Supplementary material

Supplementary data to this article can be found online at https://doi.org/10.1016/j.radonc.2024.110117.

References

[1] Makale MT, McDonald CR, Hattangadi-Gluth JA, Kesari S. Mechanisms of radiotherapy-associated cognitive disability in patients with brain tumours. Nat Rev Neurol 2017;13:52–64. https://doi.org/10.1038/nrneurol.2016.185.
[2] Coomans MB, van der Linden SD, Gehring K, Taphoorn MJB. Treatment of cognitive deficits in brain tumour patients: current status and future directions. Curr Opin Oncol 2019;31:540–7. https://doi.org/10.1097/CCO.0000000000000581.
[3] Brinkman TM, Krasin MJ, Liu W, Armstrong GT, Ojha RP, Sadighi ZS, et al. Long-term neurocognitive functioning and social attainment in adult survivors of pediatric CNS tumors: Results from the st jude lifetime cohort study. J Clin Oncol 2016;34:1358–67. https://doi.org/10.1200/JCO.2015.62.2589.
[4] Ajithkumar T, Price S, Horan G, Burke A, Jefferies S. Prevention of radiotherapy-induced neurocognitive dysfunction in survivors of paediatric brain tumours: the potential role of modern imaging and radiotherapy techniques. Lancet Oncol 2017;18:e91–100. https://doi.org/10.1016/S1470-2045(17)30030-X.
[5] Journy N, Indelicato DJ, Withrow DR, Akimoto T, Alapetite C, Araya M, et al. Patterns of proton therapy use in pediatric cancer management in 2016: An international survey. Radiother Oncol 2019;132:155–61. https://doi.org/10.1016/j.radonc.2018.10.022.
[6] Lühr A, von Neubeck C, Krause M, Troost EGC. Relative biological effectiveness in proton beam therapy – Current knowledge and future challenges. Clin Transl Radiat Oncol 2018;9:35–41. https://doi.org/10.1016/j.ctro.2018.01.006.
[7] Paganetti H. Mechanisms and Review of Clinical Evidence of Variations in Relative Biological Effectiveness in Proton Therapy. International Journal of Radiation Oncology*Biology*Physics 2022;112:222–36. https://doi.org/10.1016/j.ijrobp.2021.08.015.
[8] Eulitz J, G. C. Troost E, Klünder L, Raschke F, Hahn C, Schulz E, et al. Increased relative biological effectiveness and periventricular radiosensitivity in proton therapy of glioma patients. Radiotherapy and Oncology 2023;178:109422. doi:10.1016/j.radonc.2022.11.011.
[9] Harrabi SB, von Nettelbladt B, Gudden C, Adeberg S, Seidensaal K, Bauer J, et al. Radiation induced contrast enhancement after proton beam therapy in patients with low grade glioma – How safe are protons? Radiother Oncol 2022;167:211–8. https://doi.org/10.1016/j.radonc.2021.12.035.
[10] Bahn E, Bauer J, Harrabi S, Herfarth K, Debus J, Alber M. Late Contrast enhancing brain lesions in proton-treated patients with low-grade glioma: clinical evidence for increased periventricular sensitivity and variable RBE. Int J Rad Oncol*Biolo*Phys 2020;107:571–8. https://doi.org/10.1016/j.ijrobp.2020.03.013.
[11] Acharya MM, Green KN, Allen BD, Najafi AR, Syage A, Minasyan H, et al. Elimination of microglia improves cognitive function following cranial irradiation. Sci Rep 2016:6. https://doi.org/10.1038/srep31545.
[12] Feng X, Jopson TD, Paladini MS, Liu S, West BL, Gupta N, et al. Colony-stimulating factor 1 receptor blockade prevents fractionated whole-brain irradiation-induced memory deficits. J Neuroinflammation 2016:13. https://doi.org/10.1186/s12974-016-0671-y.
[13] Feng X, Liu S, Chen D, Rosi S, Gupta N. Rescue of cognitive function following fractionated brain irradiation in a novel preclinical glioma model. Elife 2018:7. https://doi.org/10.7554/eLife.38865.
[14] Gibson EM, Monje M. Microglia in cancer therapy-related cognitive impairment. Trends Neurosci 2021;44:441–51. https://doi.org/10.1016/j.tins.2021.02.003.
[15] Voshart D, Takuya O, Jiang Y, van der Linden G, Ainslie A, Reali Nazario L, et al. Radiotherapy induces persistent innate immune reprogramming of microglia into a primed state. Cell Reports 2024;43:113764. https://doi.org/10.1016/j.celrep.2024.113764.
[16] Wendeln A-C, Degenhardt K, Kaurani L, Gertig M, Ulas T, Jain G, et al. Innate immune memory in the brain shapes neurological disease hallmarks. Nature 2018;556:332–8. https://doi.org/10.1038/s41586-018-0023-4.
[17] Perry VH, Holmes C. Microglial priming in neurodegenerative disease. Nat Rev Neurol 2014;10:217–24. https://doi.org/10.1038/nrneurol.2014.38.
[18] Fowler JF. The linear-quadratic formula and progress in fractionated radiotherapy. Br J Radiol 1989;62:679–94. https://doi.org/10.1259/0007-1285-62-740-679.
[19] Boon SN, van Luijk P, Schippers JM, Meertens H, Denis JM, Vynckier S, et al. Fast 2D phantom dosimetry for scanning proton beams. Med Phys 1998;25:464–75. https://doi.org/10.1118/1.598221.
[20] Luijk P van, Veld AA van 't, Zelle HD, Schippers JM. Collimator scatter and 2D dosimetry in small proton beams. Phys Med Biol 2001;46:653–70. doi:10.1088/0031-9155/46/3/303.
[21] van Luijk P, Bijl HP, Coppes RP, van der Kogel AJ, Konings AWT, Pikkemaat JA, et al. Techniques for precision irradiation of the lateral half of the rat cervical spinal cord using 150 MeV protons. Phys Med Biol 2001;46:2857–71. https://doi.org/10.1088/0031-9155/46/11/307.
[22] Parente A, de Vries EFJ, van Waarde A, Ioannou M, van Luijk P, Langendijk JA, et al. The acute and early effects of whole-brain irradiation on glial activation, brain metabolism, and behavior: a positron emission tomography study. Mol Imag Biol 2020;22:1012–20. https://doi.org/10.1007/s11307-020-01483-y.
[23] Cotteleer F, Faber H, Konings AWT, Van Der Hulst PC, Coppes RP, Meertens H. Three-dimensional dose distribution for partial irradiation of rat parotid glands with 200 kV X-rays. Int J Radiat Biol 2003;79:689–700. https://doi.org/10.1080/09553000310001610268.
[24] van der Kogel AJ, Joiner MC. The dose rate effect. In: van der Kogel AJ, Joiner MC, editors. Basic Clinical Radiobiology. 5th edition. Boca Raton: CRC Press/Taylor & Francis group; 2018. p. 143–51.
[25] Robinson MD, McCarthy DJ, Smyth GK. edgeR: a Bioconductor package for differential expression analysis of digital gene expression data. Bioinformatics 2010;26:139–40. https://doi.org/10.1093/bioinformatics/btp616.
[26] Wickham H. ggplot2: Elegant Graphics for Data Analysis. New York, NY: Springer New York; 2009. doi:10.1007/978-0-387-98141-3.
[27] Kolde R. pheatmap: Pretty Heatmaps 2019.
[28] Yu G, Wang L-G, Han Y, He Q-Y. clusterProfiler: an R Package for comparing biological themes among gene clusters. OMICS 2012;16:284–7. https://doi.org/10.1089/omi.2011.0118.
[29] van Weering HRJ, Nijboer TW, Brummer ML, Boddeke EWGM, Eggen BJL. Microglia morphotyping in the adult mouse CNS using hierarchical clustering on principal components reveals regional heterogeneity but no sexual dimorphism. Glia 2023. https://doi.org/10.1002/glia.24427.
[30] Ward JH. Hierarchical Grouping to Optimize an Objective Function. J Am Stat Assoc 1963;58:236–44. https://doi.org/10.1080/01621459.1963.10500845.
[31] Holtman IR, Raj DD, Miller JA, Schaafsma W, Yin Z, Brouwer N, et al. Induction of a common microglia gene expression signature by aging and neurodegenerative conditions: a co-expression meta-analysis. Acta Neuropathol Commun 2015;3:31. https://doi.org/10.1186/s40478-015-0203-5.
[32] Lassaletta Á, Morales JS, Valenzuela PL, Esteso B, Kahalley LS, Mabbott DJ, et al. Neurocognitive outcomes in pediatric brain tumors after treatment with proton versus photon radiation: a systematic review and meta-analysis. World J Pediatr 2023. https://doi.org/10.1007/s12519-023-00726-6.
[33] Eulitz J, Troost EGC, Raschke F, Schulz E, Lutz B, Dutz A, et al. Predicting late magnetic resonance image changes in glioma patients after proton therapy. Acta Oncol (Madr) 2019;58:1536–9. https://doi.org/10.1080/0284186X.2019.1631477.
[34] Peeler CR, Mirkovic D, Titt U, Blanchard P, Gunther JR, Mahajan A, et al. Clinical evidence of variable proton biological effectiveness in pediatric patients treated for ependymoma. Radiother Oncol 2016;121:395–401. https://doi.org/10.1016/j.radonc.2016.11.001.
[35] Tang TT, Zawaski JA, Kesler S, Beamish CA, Inoue T, Perez EC, et al. Cognitive and Imaging Differences After Proton and Photon Whole Brain Irradiation in a Preclinical Model. International Journal of Radiation Oncology*Biology*Physics 2022;112:554–64. https://doi.org/10.1016/j.ijrobp.2021.09.005.
[36] Grassberger C, Paganetti H. Varying relative biological effectiveness in proton therapy: knowledge gaps versus clinical significance. Acta Oncol (Madr) 2017;56:761–2. https://doi.org/10.1080/0284186X.2017.1316516.
[37] Brown PD, Gondi V, Pugh S, Tome WA, Wefel JS, Armstrong TS, et al. Hippocampal Avoidance During Whole-Brain Radiotherapy Plus Memantine for Patients With Brain Metastases: Phase III Trial NRG Oncology CC001. J Clin Oncol 2020;38:1019–29. https://doi.org/10.1200/JCO.19.02767.
[38] Monje ML, Toda H, Palmer TD. Inflammatory blockade restores adult hippocampal neurogenesis. Science 1979;2003:1760–5. https://doi.org/10.1126/science.1088417.
[39] Lin C, Wang N, Xu C. Glioma-associated microglia/macrophages (GAMs) in glioblastoma: Immune function in the tumor microenvironment and implications for immunotherapy. Front Immunol 2023:14. https://doi.org/10.3389/fimmu.2023.1123853.